High-Frequency Surface Dynamics at an Electroactive Polymer Producing Underwater Soundwaves

Visschers, Fabian L.L.; Massaad, Jack; van Neer, Paul L.M.J.; Verweij, Martin D.; Liu, Danqing; Broer, Dirk J.

DOI
10.1002/adfm.202110754

Publication date
2022

Document Version
Final published version

Published in
Advanced Functional Materials

ADVANCED FUNCTIONAL MATERIALS
www.afm-journal.de

High-Frequency Surface Dynamics at an Electroactive Polymer Producing Underwater Soundwaves

*Fabian L. L. Visschers, Jack Massaad, Paul L. M. J. van Neer, Martin D. Verweij, Danqing Liu, and Dirk J. Broer**

Coatings with dynamic surface structures are appealing to many applications like haptics and soft robotics. Restrictively, the speed of the surface dynamics in these coatings is often limited to frequencies below 1 kHz, which makes them unsuitable for applications like acoustics and communication optics. This work describes a method to create high-frequency surface dynamics controlled by alternating electric fields on a substrate-contact-modulated coating that consists of an elastic poly(dimethyl siloxane) network supported by SU-8 microstructures. The principle is based on the global application of Maxwell stress that is locally resisted by the supporting SU-8 microstructures. In-between the microstructures the elastic material is stretched, causing a large deformation of the surface topography, which is supported by the authors' finite element method models. By applying a high-frequency alternating field, they discovered resonance effects at frequencies up to 230 kHz, where the surface of the coating vibrates at high speeds and large amplitudes. At these high frequencies, the coatings can produce and detect ultrasound waves underwater, indicating their potential for ultrasound transducers in the future.

1. Introduction

In nature, surfaces that separate organisms from their environment are often modified to perform a specific task such as self-cleaning,[1,2] (anti)-adhesion,[3–6] camouflage,[7] signaling,[8] and temperature control.[9] Inspired by nature, coatings have been developed that add dynamic properties like switchable surface morphologies in response to external stimuli like pH,[10] light,[11,12] temperature,[13,14] and electric fields.[15–20] Electric field responsive coatings in particular, have the opportunity to provide a high-frequency input, which in turn can potentially lead to a high-frequency output in terms of surface dynamics. So far however, electric-field responsive coatings have demonstrated surface dynamics that are still in the low-frequency range below 1 kHz. Coatings that would display dynamic morphologies at higher frequencies could expand the range of applications to, for instance, acoustics (non-destructive testing[21] and medical imaging[22]) and communication optics.[23] These coatings have some similarities with capacitive micromachined ultrasonic transducers (CMUTs) and piezoelectric micromachined ultrasound transducers (PMUTs) that can also generate high frequency surface dynamics. CMUTs and PMUTs however, are not suitable to coat large surfaces and require more elaborate fabrication methods like the vacuum-sealing of the membrane.[24] Previously, we have presented methods to generate dynamic surface topographies at soft viscoelastic polymer coatings.[18,19] Although we have demonstrated great control over the shape and amplitude of the formed topographies in these systems, the frequency range is still limited to a maximum of 5 Hz by the viscoelastic properties. In this context, we now present a

F. L. L. Visschers, D. Liu, D. J. Broer
Laboratory of stimuli-responsive functional materials and devices (SFD)
Department of Chemical Engineering & Chemistry
De Rondom, Eindhoven 5612 AP, The Netherlands
E-mail: D.Broer@tue.nl

F. L. L. Visschers, D. Liu, D. J. Broer
Institute for Complex Molecular Systems (ICMS)
Eindhoven University of Technology
De Rondom, 70, Eindhoven 5612 AP, The Netherlands

The ORCID identification number(s) for the author(s) of this article can be found under https://doi.org/10.1002/adfm.202110754.

DOI: 10.1002/adfm.202110754

J. Massaad, P. L. M. J. van Neer, M. D. Verweij
Laboratory of Medical Imaging
Department of Imaging Physics
Delt University of Technology
Lorentzweg 1, Delft 2628 CJ, The Netherlands

P. L. M. J. van Neer
Department of Acoustics and Sonar
TNO
Oude Waalsdorperweg 63, The Hague 2597 AK, The Netherlands

M. D. Verweij
Department of Biomedical Engineering
Thorax Center, Erasmus MC
Doctor Molewaterplein 40, Rotterdam 3015 GD, The Netherlands

D. Liu, D. J. Broer
SCNU-TUE Joint Lab of Device Integrated Responsive Materials (DIRM)
South China Normal University
Guangzhou Higher Education Mega Center
No. 378, West Waihuan Road, Guangzhou 510006, China

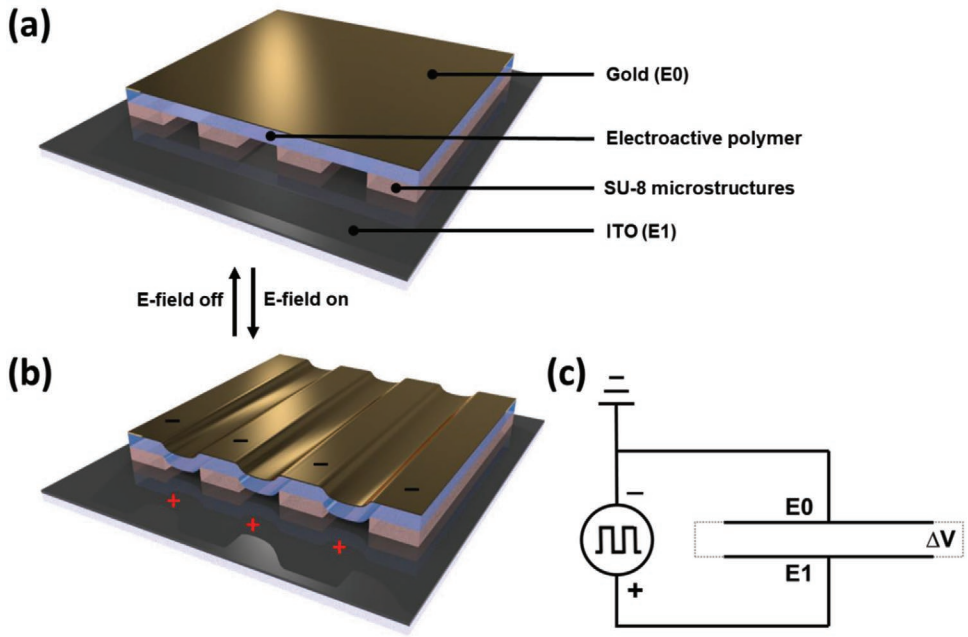

Figure 1. Design principle of an electroactive polymer coating with switchable surface topography. a) Schematic representation of the device configuration. b) After application of the electric field, the surface can alter its topography according to the programmed SU-8 structure underneath. As the pockets collapse, their content is pushed out of the sample via escape points at the edges of the samples. c) The electric circuit of the device. The electroactive polymer combined with the micro-structured SU-8 work as a two-plate capacitor when placed in the external electric field.

new method to create high-frequency surface dynamics controlled by alternating electric fields on a coating that consists of an elastic poly(dimethyl siloxane) network supported by SU-8 microstructures. Finite element method (FEM) simulations are employed to guide our experimental setup and to help with the understanding of the deformation under a DC electric field. Digital holographic microscopy (DHM) measurements are used to confirm the predicted deformations at relatively low frequencies. When using alternating electric fields, we discovered resonance effects that occur at frequencies up to 230 kHz. Controlled by the high frequency alternating electric field, the local surface vibrations demonstrate higher amplitudes and speeds than the methods we have previously presented.[18,19,25] Finally, the potential of these coatings to function as ultrasound transducers is shown by performing acoustic transmission and reception measurements underwater.

2. Results

In our method to obtain high-frequency surface dynamics, we have created SU-8 epoxide microstructures on a rigid glass substrate provided with a continuous conductive layer of indium tin oxide (ITO, E1). The microstructures support a spin coated electroactive polymer that consists of a poly(dimethylsiloxane) (PDMS) elastomer. On top of the PDMS elastomer we sputter-coated a thin layer of gold which serves as a flexible top electrode (E0). The sample design is shown in **Figure 1**a. The surface vibrations are produced by periodically induced Maxwell stresses, commonly used to compress dielectric elastomers where a thin elastomeric film is sandwiched between two flexible electrodes in a two-plate capacitor setup.[26–28] When Maxwell stresses compress the coatings, the global in-plane displacement is locally prohibited by the rigid microstructures on the substrate. In-between the microstructures however, the film can be stretched to fill the previously unoccupied space resulting in a deformation of the coating's surface (Figure 1b). As the pockets collapse, air can freely flow out of the coating via escape points at the edges of the sample. To initiate a surface deformation, the surface potentials E0 and E1 are supplied with opposite polarity indicated by ΔV in the electric circuit (Figure 1c), typically the voltage ranges from 150 to 210 V. Further details of the device preparation and dimensions are provided in the Experimental Section.

To predict the deformation mechanics and to guide our experimental setup, we schematically reproduced the design of our system in the nonlinear FEM software of Marc Mentat, using a coupled electrostatic-structural analysis.[29] The material properties of the PDMS used in the simulations were obtained with rheology by performing oscillatory frequency sweeps. The frequency dependent storage and loss modulus of the PDMS were converted into a Prony series and used as an input in Marc Mentat. In the simulations the gap distances between the microstructures are 100 µm, which is also the width of the microstructures themselves. More details can be found in Note S1, Supporting Information. Upon applying an electric field with a potential of 210 V, the surface topography changes significantly due to a partial collapse of the air pockets (**Figure 2**a,b). Directly above the microstructures, the Maxwell stresses are resisted, and no significant contraction is determined. In-between the micro-structures, only the elastic PDMS counteracts the Maxwell stress and a contraction of more than 3 µm is observed. Next, the contraction above the gap areas is calculated using various gap distances and plotted as a function of the applied potential difference (Figure 2c). The results indicate that the gap distance has a large influence on the

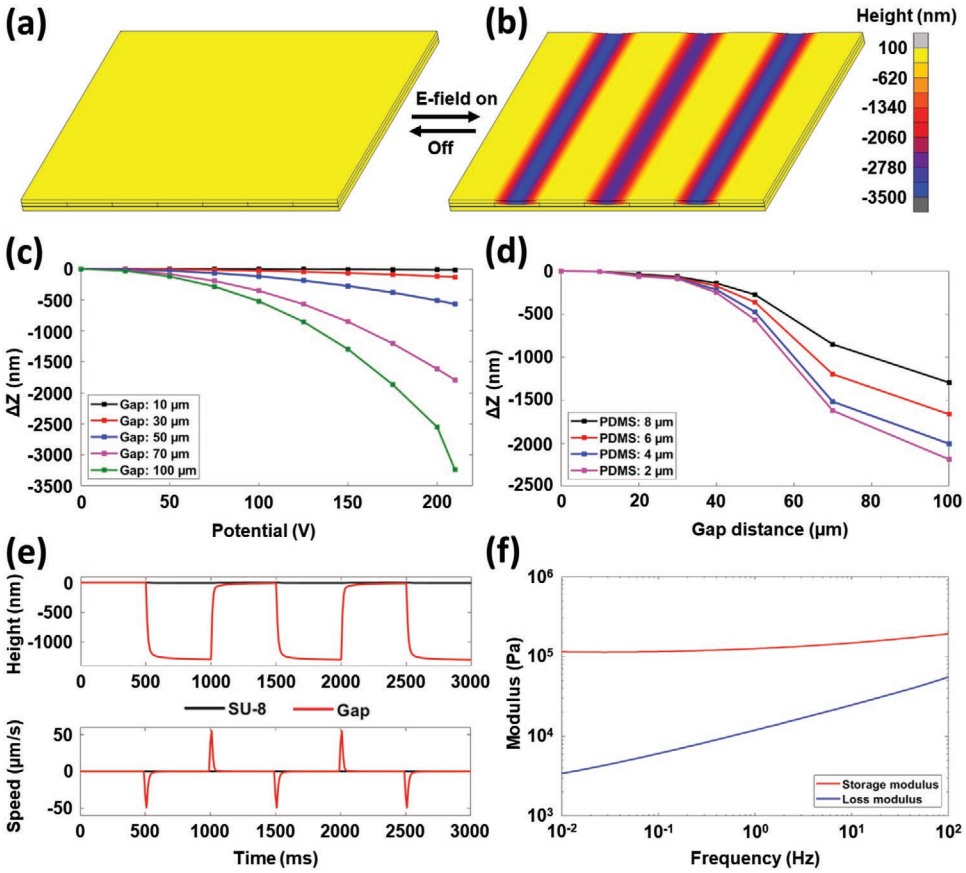

Figure 2. Simulated results of the electro-mechanical surface dynamics. Simulated 3D images showing a) the initial coating surface and b) the actuated coating surface when subjected to an electric field at a DC potential of 210 V. c) Influence of the applied potential difference on the deformation amplitude at various gap distances. d) Influence of the gap distance on the deformation amplitude using various thicknesses of the elastic PDMS at DC potentials of 150 V. e) The predicted change in surface height and deformation speed above the SU-8 (black) and above the gap area (red). The gap distance is 100 µm and the electric field switches at a frequency of 1 Hz between 0 and 150 V. f) Measured storage modulus G′ and loss modulus G″ when the coating is subjected to a frequency sweep at 5% strain.

magnitude of the contraction. This effect is explained by the decrease of the elastic counterforce as the gap distance between the microstructures increases. On top of that, a larger gap distance increases the effective surface area where the Maxwell stress is applied, which results in a larger compressive force. To continue our analysis, we simulate how the thickness of the PDMS top film affects the contraction occurring at several different gap distances (Figure 2d and Movie S1, Supporting Information). In these simulations the applied potential difference is lowered from 210 to 150 V, to prevent compilation errors that occur when large strains are generated. The results indicate that a thinner PDMS layer results in a larger contraction, which is explained by the increase in the electric field strength as well as by the decrease in elastic counterforce. At large gap distances, the flattening of the curves in Figure 2d is most likely caused by the geometrical constraints of the system where the maximum deformation is limited to 8 µm by the height of the gap. Moving forward, we use the developed model for predicting the kinetics of the surface dynamics. The surface is brought into motion using an alternating electric field at a frequency of 1 Hz with a peak-to-peak potential difference of 150 Vpp. The simulated response of the coating is monitored as a function of time at two adjacent locations: above the SU-8 and above the gap (Figure 2e). The simulations predict a height difference of more than 1 µm occurring at a maximum speed of 50 µm s^{-1}. The quick response of the coating to the alterations in the electric field indicates that the elastic properties of the material control the deformation. The fast elastic response is expected as the frequency-dependent storage (G′) and loss (G″) moduli, which were used to describe the viscoelastic properties in the FEM model, do not indicate the presence of a strong viscous component (Figure 2f). More details can be found in Note S2, Supporting Information.

The FEM simulations predict response times of less than 100 ms and surface deformations of several micrometers for this new coating design. Now, the proposed actuation principle is demonstrated experimentally by monitoring the surface deformation using DHM measurements. Prior to actuation, the coating surface shows a small relief matching the shape of the SU-8 microstructures underneath, which is a result of the fabrication process (**Figure 3**a,c [black curve] and Movie S2, Supporting Information). Upon applying the electric field with a potential of 210 V, the air pockets in-between the SU-8 microstructures partially collapse resulting in a large surface

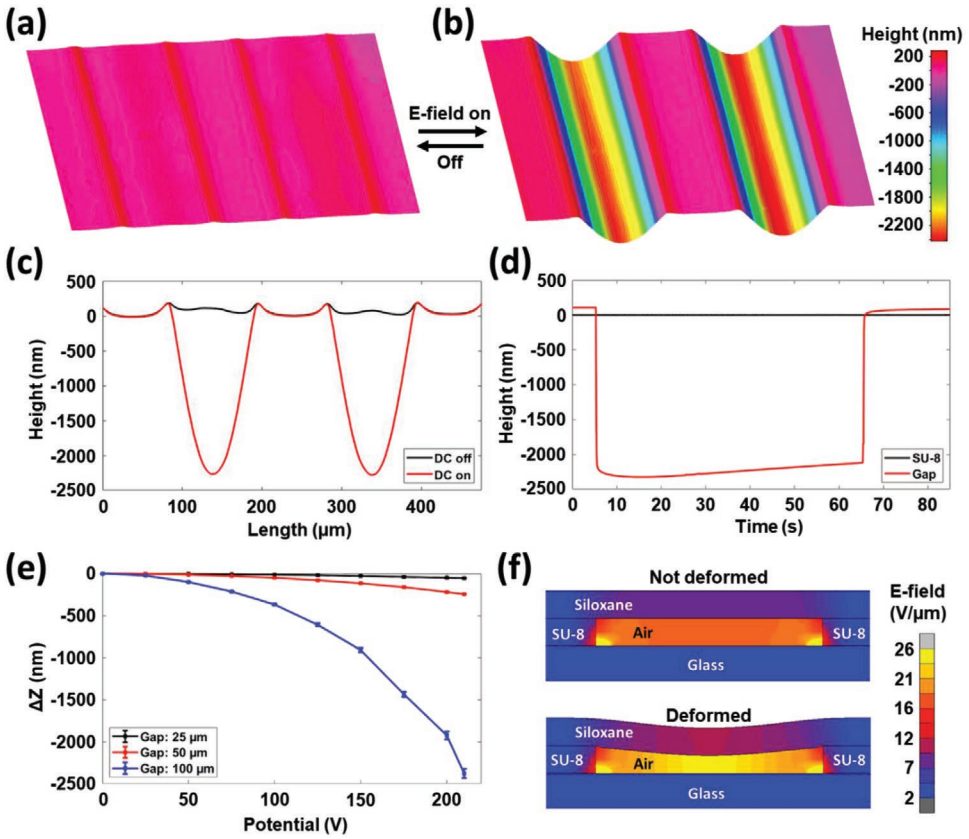

Figure 3. Details of the electro-mechanical surface deformation. 3D images measured by DHM show a) the small surface relief without electric field and b) the surface of the coating when subjected to an electric field at a DC potential of 210 V. c) The corresponding 2D profile of Figure 3a,b. The black curve shows the surface profile without electric field, while the red curve is measured when the electric field is applied. d) Measured change of the surface height above the SU-8 (black) and above the gap area (red). e) Influence of the electric field strength on the contraction above the gap area for microstructures with various gap distances. The error bars indicate the standard deviation of the measurements. f) The results from FEM simulations of the electric field distribution in cross sections of the coating. The top image shows the electric field distribution in the original shape, while the bottom image shows how the field distribution changes as the coating deforms.

deformation with contraction of more than 2 µm (Figure 3b,c [red curve]). Next, we further analyze the surface deformation by extracting the time-resolved electro-mechanical response of the coating at two adjacent locations (Figure 3d). The first location is positioned directly above the SU-8 material, while the second location is placed above the center of the gap area. The initial deformation occurs fast with a slight overshoot that takes a few minutes to equilibrate. The long equilibration time, compared to the fast initial surface deformation, is caused by the interplay between the Maxwell stress and the elastic counterforce. During the overshoot, the electric field strength in the gap area increases significantly because the top and bottom electrodes draw closer (Figure 3f). As a result, the Maxwell stress also increases and works against the elastic counter force, which prolongs the equilibration process of the surface deformation. To continue the analysis of the deformation, the influence of the gap distance in-between the microstructures is also determined at various DC potentials (Figure 3e). As predicted by our FEM simulations, adjusting the geometry of the microstructures has a large impact on the maximum contraction of the surface, because the geometry determines the length of the elastomer that can be deformed.

Next, the kinetics of the surface dynamics are extracted from the time resolved DHM measurements. First, the surface is brought into a vibrating motion using a pulse generator at a frequency of 1 Hz with a peak-to-peak potential difference of 150 Vpp, similar to our FEM simulation. Two key locations above the SU-8 and the center of the gap are tracked while monitoring the applied electric field (**Figure 4**a). A qualitative comparison between the experimental results from Figure 4a and simulated results from Figure 2e shows that in both cases the surface reacts with a rapid elastic-like deformation upon switching of the electric field. Height differences of more than 800 nm are measured at a maximum deformation speed of 20 µm s^{-1}. Interestingly, both experimental and simulated results show that the return of the coating to its original shape occurs faster than the initial deformation. This effect is caused by the instant release of the stored elastic energy in the coating when the pressure from the electric field is removed. Subsequently, the surface vibrations are measured during a frequency sweep, where the amplitude of the vibration is plotted as a function of the frequency of the input signal (Note S3 and Figure S2, Supporting Information). To find out the resonance frequency of the device, the Fast Fourier transformation (FFT) of each output signal is calculated, and their respective Fourier

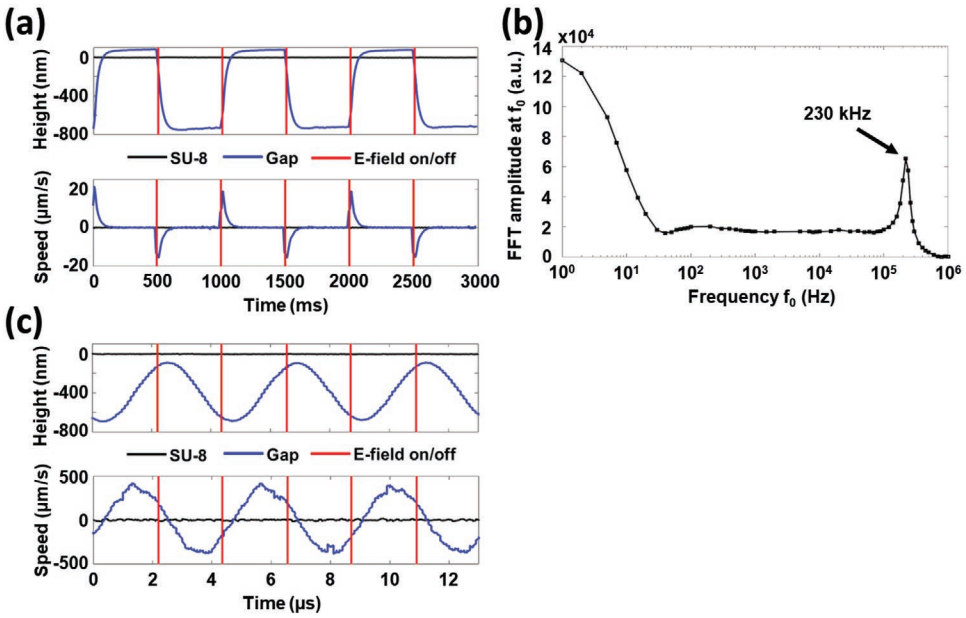

Figure 4. DHM measurements from electric field induced surface vibrations. a) The change in surface height and deformation speed using an AC potential of 150 Vpp at a frequency of 1 Hz. The gap distance is 100 µm. Vertical red lines indicate the moments the electric field switches on or off. b) Amplitude of the Fourier coefficient of each measured signal at $f = f_0$. c) The change in surface height and deformation speed using an AC potential of 150 Vpp at a frequency of 230 kHz.

coefficient at $f = f_0$, with f_0 being the excitation frequency of the input signal is determined (Figure 4b), which clearly indicates a resonant behavior as the amplitude of the coefficient reaches a peak at 230 kHz. A more detailed analysis of the surface vibration at the resonance frequency of 230 kHz, reveals a sine shaped temporal motion of the PDMS film (Figure 4c). The obtained deformation amplitude is 600 nm, which is generated at a maximum speed of almost 500 µm s^{-1}. In comparison, we achieved maximum surface displacement speeds of 5 µm s^{-1} in our previously described systems, where we used softer PDMS with a lower crosslinking density and no SU-8 micro structuring.[18] The position of the resonance peak is anticipated to be determined by the geometric constraints of the microstructure and the thickness and modulus of the PDMS film. Future experiments are planned to further tune the fundamental frequency by altering these parameters.

Next, to demonstrate the high speeds at which the surfaces of the coatings vibrate, and to explore their potential for transducer applications, they are placed underwater to perform acoustic measurements in transmission and in reception. In underwater acoustics, it is common to characterize the performance of a specific sensor by measuring its transmit and receive transfer function, also known as efficiency and sensitivity, respectively. Usually, the efficiency is determined by computing, in the Fourier domain, the ratio between the acoustical pressure measured by the hydrophone and the input voltage on the PDMS sample.[30] In this case however, when a 1-cycle sine wave with a center frequency of f_0= 230 kHz (150 Vpp) is used as an input signal on the sample (**Figure 5**a), the received signal shows amplitude peaks at $2f_0$ and $4f_0$ (Figure 5b,c). The same behavior was observed with an excitation frequency of f_0 = 650 kHz. The occurrence of the amplitude peaks at $2f_0$ and $4f_0$ is explained by the compression force exserted on the coating, which is always positive regardless of a positive or negative input potential. As a result, a rectifying effect takes place in the deformation, which doubles the input frequency of the main component of the force, accompanied by smaller components with higher even multiples of the input frequency. Despite the rectifying effect in the deformation of the coating, there is no DC component in the generated pressure. This DC component is effectively removed by the double time derivative linking the produced acoustic pressure and the volume injection rate induced by the membrane displacement. Since the rectifying effect is nonlinear, the performance of the sample is not determined by the conventional computation of the transmit transfer function, which is based on a linear system theory. Instead, we calculated the generated pressure and displacement at the surface of the coating as an indication of its resonance frequency in water. Details of the calculations of the pressure and displacement at the surface of the coatings are described in Note S4, Supporting Information. To further investigate the relationship between transmitted and received center frequency, a half-cycle pulse (with a non-zero DC component) was used as input signal (Figure 5d). Since the half-cycle excitation is positive in sign, no rectifier effect is expected. The received signals for the three different input peak voltages (37.5, 75, and 150 V) and excitation frequencies of 230 kHz are detected with a delay of 132 µs (Figure 5e) and amplitude peaks at $3f_0$ (Figure 5f). The signals obtained from excitation frequencies of 460 and 690 kHz show similar results (Note S5 and Figure S3, Supporting Information). Next, the pressure (Figure 5g) and displacement (Figure 5h) at the surface of the coating are calculated from the signals with excitation frequencies of 230 kHz. The computed signals at excitation frequencies of 460 and 690 kHz show lower amplitudes (Note S6 and Figure S4, Supporting

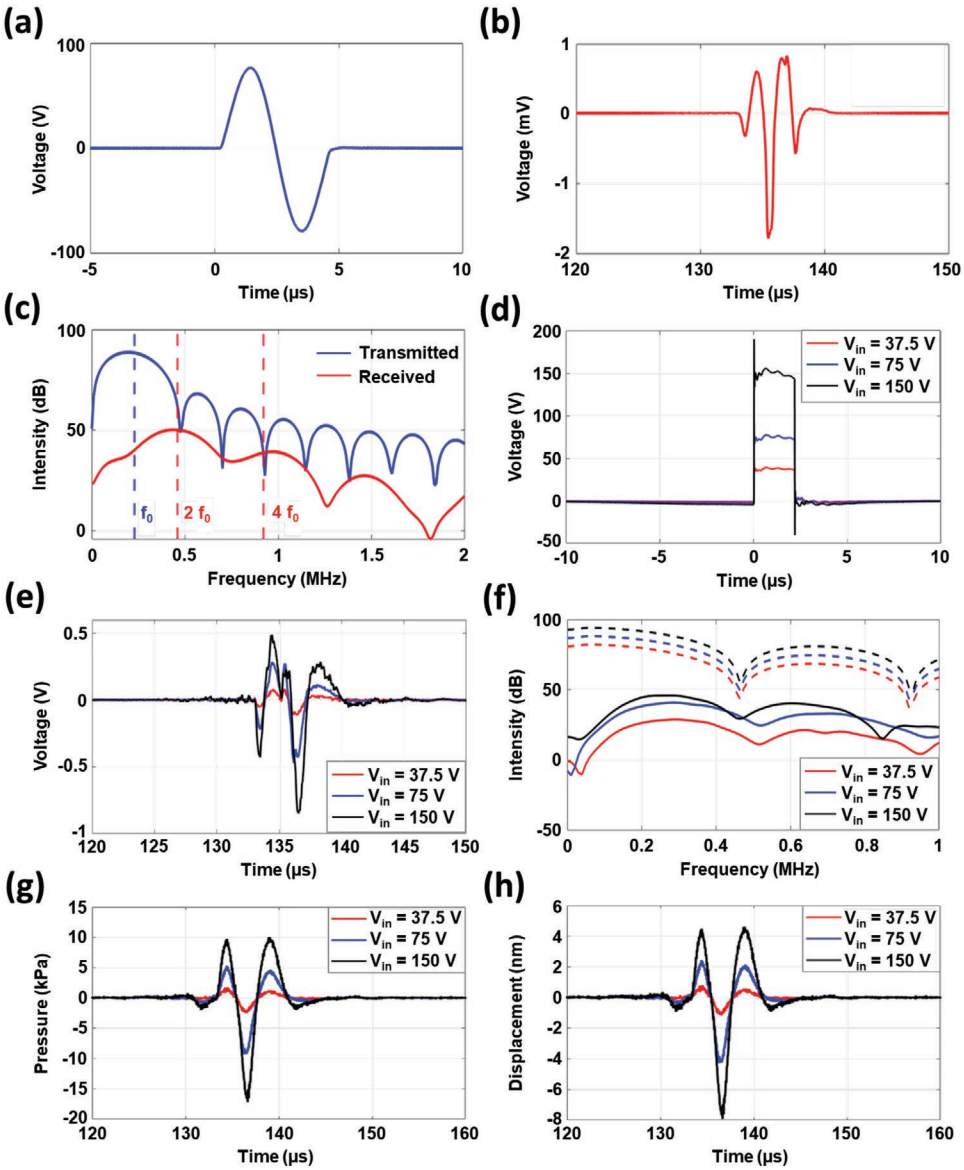

Figure 5. Acoustic characterization underwater. a) Initial input signal on the coating. b) Signal measured by the hydrophone when using the input signal from Figure 5a. c) Magnitude of the Fourier Transform of the signal from Figure 5a,b. d) Input signals on the coating that consist of a half cycle pulse at a frequency of 230 kHz and different amplitudes. e) Signals measured by the hydrophone when using the input signals from Figure 5d. f) Magnitude of the Fourier Transform of the signal from Figure 5d (dotted lines) and 5e (continuous lines). Pressure (g) and displacement (h) signals at the surface of the coatings, while excited with a half cycle pulse at a frequency of 230 kHz.

Information). The shape and frequency content of these signals are as expected considering the shape of the input signal (a half-cycle square pulse) and the fact that the ultrasound transducer analyzer (Verasonics) adds one extra wavelength to the excitation waveform. The calculated signals indicate that the sample performs best at 230 kHz, the same as in air, despite the large acoustic impedance difference between air (1 Rayl) and water (1.5 MRayl). Also, because of this large difference, lower surface displacements in water are expected and indeed measured (maximum of 8 nm with a pressure of 17 kPa) due to the $\approx 10^6$ heavier load the coating needs to displace in water relative to air. These displacements were approximately two orders of magnitude lower than those measured in air.

Finally, to further investigate the applicability of the coatings in sound transducers, we explore their potential to also receive sound signals underwater. A calibrated source with a half-cycle square pulse and a center frequency f_0 of 230 kHz is used as an input signal, which will produce a sinusoidal like pressure pulse impinging on the coating. The initial amplitude of the input signal is set to a peak voltage of 150 V, producing an acoustic pressure of 400 kPa at the surface of the calibrated source. The coating, placed at a distance of 120 mm from the calibrated source, receives the signal after a delay of 80 µs (**Figure 6**a) with a fundamental frequency also centered around f_0 (Figure 6b). Thus, the high-frequency-like characteristic observed in the signals from Figure 6a are not associated to noise, but rather

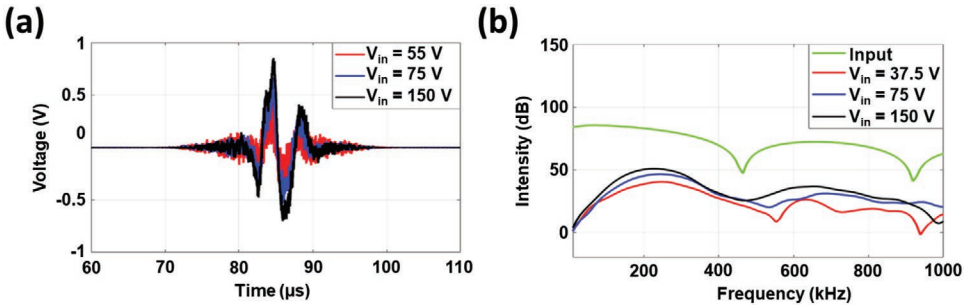

Figure 6. a) Signals measured by the coating at a distance of 120 mm from a calibrated source, with a half-cycle square pulse at a frequency of 230 kHz. b) Magnitude of the Fourier Transform applied on the signals received by the coating.

inconsistencies in the coating. The rectifying effect does not occur here, and the device behaves as a freely vibrating membrane in reception. More details can be found in Note S7, Supporting Information. The results indicate that the coatings indeed have the capability to transmit and detect sound waves underwater. Still, the performance is about 10 times lower than typical underwater transducers,[30–33] although there are some practical measures to improve this further. For instance, the receive transfer function could be increased by reducing the gap height and coating thickness, which will increase the electrostatic effect. Similar to CMUTs and PMUTs, the device can be optimized for transmission (large gap heights) and reception (small gap heights and limited dynamic range).

3. Conclusion

In conclusion, we have developed a new method to obtain large topographical changes at the surface of a substrate-contact-modulated coating under a DC electric field, as well as high-frequency surface vibrations triggered by an AC electric field. Our approach is based on the generation of Maxwell stresses in a film supported by SU-8 microstructures. The air pockets in-between the micro-structures can partially collapse under the pressure from the electric field, resulting in a large change of the surface topography, as supported by FEM simulations. When using AC electric fields, the surface vibrates and a fundamental frequency is discovered at 230 kHz. The obtained deformation amplitude of 600 nm is reached at a speed of more than 400 µm s^{-1}. The fabricated PDMS coating is also able to transmit and receive ultrasonic waves underwater, although its performance is not yet at the same level as commercial underwater transducers. Due to the combination of high-frequency vibrations and large deformation amplitudes, we anticipate that, after some optimization, the coatings are useful in applications ranging from haptics and acoustics to microfluidics and optics. Future research is focused on obtaining control over the position of the resonance frequency and improving its acoustical response to achieve a performance that is more comparable to current ultrasound transducers.

4. Experimental Section

Finite Element Method Simulations: The electric field induced surface deformations of the coating were simulated in 3D using Marc Mentat 2014.0.0.

Materials: Glass substrates with a continuous ITO electrode were obtained from GemTech Optoelectronics. The poly(dimethyl-siloxane) (PDMS) elastomer and curing agent (Sylgard 184) were obtained from Dow Corning. The SU-8 2010 microresist was obtained from MicroChem.

Sample Preparation: The PDMS curing agent was added to the silicone elastomer in a ratio of 1:10 (as recommended by the manufacturer) to obtain a flexible elastomer network. After thorough mixing of the two components, the trapped air in the sample was removed under reduced pressure. The substrates with the ITO electrode (100 nm thickness) were cleaned by ultrasonication for 20 min in acetone and isopropanol, respectively, and dried with airflow. Subsequently, the clean substrates were subjected to a UV-ozone treatment for 20 min. The SU-8 2010 was applied on the substrates by spin coating first at 500 rpm (acceleration rate 100 rpm s^{-1}) for 5 s and then at 4000 RPM (acceleration rate 300 rpm s^{-1}) for 30 s, which resulted in a thickness of 9 µm. After a softbake of 10 min at 95 °C, the sample was exposed to UV light through a photomask at 10 mW cm^{-2} for 12.5 s. Next, the PDMS mixture was applied on the substrates by spin coating at 7000 rpm (acceleration rate 1000 rpm s^{-1}) for 2 min, which resulted in a thickness of 7 µm. The samples were then heated to 95 °C for 1 h for the curing of the PDMS and the post-exposure bake of the SU-8. After the post-exposure bake, the samples were developed in propylene glycol monomethyl ether acetate for 3 days. A thin layer of gold (10 nm) was sputter coated on top of the PDMS layer at a current of 65 mA for 11 s.

Characterization in Air: The alternating electric field with a square pulse function was provided by a function generator (Tektronix AFG3252). The electric signal from the function generator was then amplified with an amplifier (Falco Systems WMA-300). The DC potential difference was generated by a DC Power Supply (3B Scientific U33000). The output voltage was measured with an oscilloscope (Keysight InfiniiVision DSO-X 3032T). The surface topographies were measured with a Digital Holography Microscope (Lyncée Tec.). The thickness of samples was measured by an interferometer (Fogale Nanotech Zoomsurf). The mechanical properties of PDMS were measured with an oscillatory frequency sweep by a rheometer (AR-G2, TA instruments) with a strain of 5%.

Characterization Underwater: The samples were excited with half-cycle square pulses with center frequencies of 230 kHz and higher, or single sine pulses with frequencies of 230 kHz, using an arbitrary waveform generator (AWG; Agilent 33521A, Keysight Technologies, Santa Rosa, CA, USA). The input peak voltage was increased to 150 V using a 55 dB amplifier (2100L RF Amplifier, Electronic Navigation Industries, Rochester, NY, USA). The underwater signals were detected with a 1 mm-diameter calibrated hydrophone (Precision Acoustics Ltd., Dorchester, UK), which was placed in the water tank 200 mm away from the surface of the sample, at the far-field of the generated acoustic wavefield. The signal recorded by the hydrophone was amplified by a 60 dB low-noise amplifier (MITEQ, Hauppauge, NY, USA) before being finally recorded. The analysis of the signals was performed using a Verasonics ultrasound system. During the reception measurements, a 40 mm diameter 250 kHz transducer (IMASONIC 13 579 SN1006, Voray-sur-l'Ognon, FR) was used as a calibrated source to excite acoustic waves and in this setup the coating was placed at a distance of 120 mm.

Supporting Information

Supporting Information is available from the Wiley Online Library or from the author.

Acknowledgements

The results presented are part of research programs financed by the Dutch Research Council (NOW), Klein project: OCENW. KLEIN.345, and Startup project: STU.019.007.

Conflict of Interest

The authors declare no conflict of interest.

Data Availability Statement

The data that support the findings of this study are available from the corresponding author upon reasonable request.

Keywords

AC electric fields, acoustics, dynamic surfaces, Maxwell stresses, PDMS, SU-8

Received: October 23, 2021
Revised: January 27, 2022
Published online:

[1] C. Neinhuis, W. Barthlott, *Ann. Bot.* **1997**, *79*, 667.
[2] R. Fürstner, W. Barthlott, C. Neinhuis, P. Walzel, *Langmuir* **2005**, *21*, 956.
[3] L. Q. Ren, S. J. Wang, X. M. Tian, Z. Q. Han, L. N. Yan, Z. M. Qiu, *J. Bionic Eng.* **2007**, *4*, 33.
[4] Y. Tian, N. Pesika, H. Zeng, K. Rosenberg, B. Zhao, P. McGuiggan, K. Autumn, J. Israelachvili, *Proc. Natl. Acad. Sci. USA* **2006**, *103*, 19320.
[5] K. Autumn, Y. A. Liang, S. T. Hsieh, W. Zesch, W. P. Chan, T. W. Kenny, R. Fearing, R. J. Full, *Nature* **2000**, *405*, 681.
[6] R. Leach, *Characterisation of Areal Surface Texture* (Ed: R. Leach), Springer, Teddington **2013**.
[7] J. Teyssier, S. V. Saenko, D. Van Der Marel, M. C. Milinkovitch, *Nat. Commun.* **2015**, *6*, 6368.
[8] H. C. Hoch, R. C. Staples, B. Whitehead, J. Comeau, E. D. Wolf, *Science* **1987**, *235*, 1659.
[9] L. B. Pérez-Estrada, Z. Cano-Santana, K. Oyama, *Tree Physiol.* **2000**, *20*, 629.
[10] Z. Dang, L. Liu, Y. Li, Y. Xiang, G. Guo, *ACS Appl. Mater. Interfaces* **2016**, *8*, 31281.
[11] G. Babakhanova, H. Yu, I. Chaganava, Q. H. Wei, P. Shiller, O. D. Lavrentovich, *ACS Appl. Mater. Interfaces* **2019**, *11*, 15007.
[12] D. Liu, D. J. Broer, *Angew. Chem., Int. Ed.* **2014**, *53*, 4542.
[13] Q. Hao, W. Li, H. Xu, J. Wang, Y. Yin, H. Wang, L. Ma, F. Ma, X. Jiang, O. G. Schmidt, P. K. Chu, *Adv. Mater.* **2018**, *30*, 1705421.
[14] B. Wang, X. Xue, X. Liu, P. Neuzžil, B. Ma, W. Yuan, J. Luo, C. Jiang, *Appl. Mater. Today* **2018**, *13*, 271.
[15] D. Liu, N. B. Tito, D. J. Broer, *Nat. Commun.* **2017**, *8*, 1526.
[16] D. Pyo, S. Ryu, K. U. Kyung, S. Yun, D. S. Kwon, *Appl. Phys. Lett.* **2018**, *112*, 061902.
[17] S. Shian, D. R. Clarke, *Soft Matter* **2016**, *12*, 3137.
[18] F. L. L. Visschers, H. Gojzewski, G. J. Vancso, D. J. Broer, D. Liu, *Adv. Mater. Interfaces* **2019**, *6*, 1901292.
[19] F. L. L. Visschers, D. J. Broer, D. Liu, *Proc. SPIE* **2020**, *11375*, 11375F-1.
[20] E. M. Henke, K. E. Wilson, I. A. Anderson, *Bioinspiration Biomimetics* **2018**, *13*, 046009.
[21] S. K. Dwivedi, M. Vishwakarma, P. A. Soni, *Mater. Today Proc.* **2018**, *5*, 3690.
[22] A. P. Sarvazyan, M. W. Urban, J. F. Greenleaf, *Ultrasound Med. Biol.* **2013**, *39*, 1133.
[23] V. Sasikala, K. Chitra, *J. Opt.* **2018**, *47*, 307.
[24] M. S. Salim, M. F. Abd Malek, R. B. W. Heng, K. M. Juni, N. Sabri, *J. Med. Ultrasound* **2012**, *20*, 8.
[25] F. L. L. Visschers, D. J. Broer, D. Liu, *Soft Matter* **2021**, *17*, 7247.
[26] R. Pelrine, R. Kornbluh, Q. Pei, J. Joseph, *Science* **2000**, *287*, 836.
[27] S. Michel, X. Q. Zhang, M. Wissler, C. Löwe, G. Kovacs, *Polym. Int.* **2010**, *59*, 391.
[28] R. E. Pelrine, R. D. Kornbluh, J. P. Joseph, *Sens. Actuators A* **1998**, *64*, 77.
[29] MSC Software Corporation (2014): Theory and User Information, Vol. *A*, MSC Software Corporation, Newport Beach, California **2014**.
[30] P. L. M. J. van Neer, G. Matte, J. Sijl, J. M. G. Borsboom, N. de Jong, *Ultrasonics* **2007**, *46*, 336.
[31] P. L. M. J. van Neer, G. Matte, M. G. Danilouchkine, N. de Jong, C. Prins, F. van den Adel, *IEEE Trans. Ultrason., Ferroelectr., Freq. Control* **2010**, *57*, 455.
[32] H. J. Vos, M. E. Frijlink, E. Droog, D. E. Goertz, G. Blacquiere, A. Gsolf, N. De Jong, A. F. W. Van Der Steen, *IEEE Ultrason. Symp.* **2004**, *3*, 1966.
[33] H. J. Vos, M. A. Frijlink, E. Droog, D. E. Goertz, G. Blacquiere, A. Gisolf, N. De Jong, A. F. W. Van Der Steern, *IEEE Trans. Ultrason., Ferroelectr., Freq. Control* **2005**, *52*, 2418.